Morphology of liquid microstructures on chemically patterned surfaces

Anton A. Darhuber, Sandra M. Troian,[a)] and Scott M. Miller
Department of Chemical Engineering, Princeton University, Princeton, New Jersey 08544

Sigurd Wagner
Department of Electrical Engineering, Princeton University, Princeton, New Jersey 08544

We study the equilibrium conformations of liquid microstructures on flat but chemically heterogeneous substrates using energy minimization computations. The surface patterns, which establish regions of different surface energy, induce deformations of the liquid–solid contact line. Depending on the geometry, these deformations either promote or impede capillary breakup and bulge formation. The contact angles of the liquid on the hydrophilic and hydrophobic regions, as well as the pattern geometry and volume of liquid deposited, strongly affect the equilibrium shapes. Moreover, due to the small scale of the liquid features, the presence of chemical or topological surface defects significantly influence the final liquid shapes. Preliminary experiments with arrays of parallel hydrophilic strips produce shapes resembling the simulated forms. These encouraging results provide a basis for the development of high resolution lithography by direct wet printing. © *2000 American Institute of Physics.* [S0021-8979(00)06211-3]

I. INTRODUCTION

During the past decade several attempts have been made at finding alternatives to photolithography for the efficient and inexpensive production of micron-sized patterns.[1–6] In microcontact printing,[1,2] a patterned polymer stamp is used to transfer a substance which forms a self-assembled monolayer onto a metal coated surface. The pattern is subsequently transferred to the metal layer by selective chemical etching. Submicron resolution has been demonstrated.[2,5] The resolution limiting factor is reported to be diffusion of ink-molecules away from the regions of contact between the stamp and the metal surface.[5] Mikami *et al.*[3] have introduced a gravure offset printing technique, which consists of transferring an ink from the grooves of an etched glass plate via a silicone roller onto a glass substrate. Fully functional electronic devices have been fabricated with this method.[3]

The optimization of the direct printing process of electronic structures requires knowledge and understanding of the equilibrium shape conformations of liquids on patterned surfaces.[7] For liquid features in the micron range, the surface to volume ratio is exceedingly large. Thus, the energetics associated with the boundary surface and interfaces determine the overall shape and stability of liquid microstructures.[8–10] These in turn are the key factors influencing the achievable edge resolution and pattern fidelity.

In this article, we examine morphological aspects of microfluid droplets deposited on flat but chemically patterned substrates, which are critical for technological applications. The patterned surfaces function as the printing plates, whose ink patterns can be transferred to a target substrate by direct contact. The ink pattern definition on the printing plate is achieved by selectively patterning the surface into hydrophilic and hydrophobic regions. A hydrophilic ink for instance will avoid the hydrophobic patches but easily adhere to the hydrophilic ones. In general, the ink may consist of several constituents, which after transfer and further processing can be used as an etch mask or component of an electronic circuit.

In what follows we present numerical simulations of the equilibrium profiles of liquid microstructures for various boundary conditions and geometrical surface patterns. We compare these computed profiles with experimental profiles of glycerol on patterned silicon wafers, where the chemical modulation was defined with a self-assembled monolayer of octadecyl-trichlorosilane (OTS).

II. EXPERIMENTAL PROCEDURE

The samples were prepared from [001]-oriented *p*-type doped silicon wafers using optical lithography. The wafers were first cleaned by immersion in a solution of concentrated H_2SO_4 and H_2O_2 (volume ratio of 7 to 3) at $90\,°C$ for 30 min, thoroughly rinsed in ultrapure, de-ionized water (18 MΩ) and then coated with a self-assembled monolayer of OTS.[11] The silane groups of the OTS molecules react with the native SiO_2 layer of the silicon surface forcing the hydrophobic alkane tails to orient in the opposite direction, thus producing a uniform hydrophobic surface. The contact angles of glycerol and water on OTS were measured to be $95°\pm3°$ and $112°\pm3°$, respectively, in close agreement with previous measurements.[12]

The next process step was the definition of a surface pattern via exposure of the OTS layer through a chromium mask on a fused silica glass substrate with intense ArF laser radiation (wavelength $\lambda=193$ nm, pulse energy $E=28$ mJ, pulse rate $f=9$ Hz) for 11 min. The UV light induces breakage of the bonds between the OTS molecules and the SiO_2 surface,[13] effectively removing the OTS from exposed re-

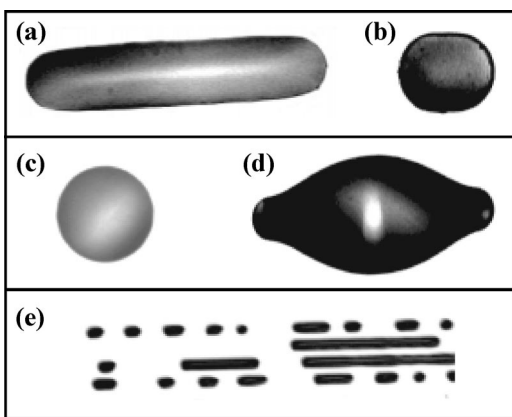[a)]Author to whom correspondence should be addressed; electronic mail: stroian@princeton.edu

J. Appl. Phys., Vol. 87, No. 11, 1 June 2000

Darhuber *et al.*   7769

FIG. 1. Top-view photographs of glycerol droplets residing on hydrophilic SiO$_2$ channels of an OTS coated silicon wafer. The widths of the structures are about (a), (b) 15 μm, (c) 10 μm, (d) 47 μm, and (e) 15 μm. The withdrawal speed of the patterned wafer from a glyercol reservoir was 10000 μm/s in (a)–(d) and 250 μm/s in (e). The slower speed results in smaller attached volumes and accelerated capillary breakup.

gions. Water droplets completely wet the exposed regions ($\theta_{H_2O} \approx 0°$) corresponding to a completely hydrophilic surface. When the exposed surface is left open to the air, however, θ_{H_2O} increases slowly over a period of several days due to adsorption of contaminants. Storage in pure, de-ionized water forestalls organic contamination. Since the monolayer film thickness formed by this procedure has been measured to be less than 3 nm,[12] the vertical height modulation of a processed surface is three orders of magnitude smaller than the lateral length scales under consideration. The surface containing the patterned OTS layer can therefore be regarded as a flat and chemically heterogeneous surface, irrespective of its nanoscopic morphology.

The experimental pattern consisted of vertical hydrophilic strips several millimeters in length and 7–15 μm in width, with a neighboring distance varying between 3 and 5000 μm. The glycerol (Aldrich Chemical Co., spectrophotometric grade) was deposited onto the patterned wafer via a dip coating technique. The wafer was immersed in glycerol and withdrawn at constant vertical speed ranging from 250 to 10 000 μm/s. Lower withdrawal rates resulted in smaller deposited volumes in accordance with similar behavior on chemically homogeneous substrates.[14]

Since the contact angle of glycerol on SiO$_2$ was measured to be less than 5°, it is classified as a wetting liquid on the UV exposed regions. Consequently, the glycerol adhered only to the SiO$_2$ lines except for regions where the line spacing was small and coalescence of neighboring glycerol lines was observed. Glycerol is a suitable liquid for these studies because of its low vapor pressure (about 0.07 Pa at 20 °C),[15] high surface tension (0.0634 N/m at 20 °C)[15] and large contact angle contrast (~90°) between the SiO$_2$ and OTS coated regions. Since glycerol is a hygroscopic liquid, the viscosity may have been lower than the nominal value for pure glycerol.

Figure 1 shows five equilibrium shapes of liquid microstructures formed within the hydrophilic SiO$_2$ channels of a patterned surface 24 h after dipping. The width of the micro-

structures varies between 10 and 47 μm. The images were recorded with a conventional optical microscope equipped with a charge coupled device camera. The various gray scales result from different focusing conditions, image contrast and brightness settings, preventing any conclusion about the height profiles in the individual frames. The samples shown in Figs. 1(a)–1(d) were withdrawn at a rate of 10 000 μm/s, while that in Fig. 1(e) was withdrawn at 250 μm/s. The liquid lines containing smaller deposited volume underwent capillary breakup much more rapidly leading to the collinear droplet arrays shown in Fig. 1(e). The samples withdrawn at higher speed remained as stable continuous lines for a period exceeding 7 h. The deposition volume, therefore, has a decisive influence on the stability of liquid microstructures and onset time for capillary breakup as will be discussed in Sec. III.

When the patterned wafers are initially withdrawn from the reservoir, continuous lines of glycerol are observed along the entire length of SiO$_2$ lanes. After exposure to air, however, evaporation and contamination by ambient dust particles or aerosolized organics promote capillary breakup. Visual inspection of isolated drops and line segments through an optical microscope revealed that droplets are preferably observed in the immediate vicinity of microscopic inhomogeneities on the surface. Conversely, the presence of these defects can be inferred from the asymmetric and perturbed shapes of the liquid–solid contact lines. We succeeded in forming continuous and stable liquid lines by minimization of the time between the UV patterning process and the surface deposition and by storage of the already patterned wafers under ultrapure water and drying them with nitrogen gas before initiating the dip-coating procedure.

In Sec. III, we present energy minimization calculations to confirm the variety of liquid shapes obtained experimentally and to predict important features of equilibrium shapes based on the surface energies, the pattern geometry and the liquid volume.

III. NUMERICAL SIMULATIONS

The numerical simulations were performed using SURFACE EVOLVER,[16] a program that minimizes the total energy of liquid structures subject to various boundary conditions and constraints. The total energy per unit area includes the surface tension γ_{lv}, the liquid–solid interfacial tension γ_{sl}, and the solid–vapor interfacial tension γ_{sv}. Gravity is neglected in these computations since the Bond number is less than 10^{-4}. The Bond number is defined as Bo = $\rho g R^2 / \gamma_{lv}$, where ρ is the liquid density and R the characteristic size of a liquid feature, which for the systems described is of order 1–10 μm. We neglect line tension in our calculations because of the large discrepancies in the literature[17] concerning both the sign and magnitude of the force, especially for liquid on solid systems. The influence of disjoining pressure or double layer forces has been implicitly included in the simulations in as much as the surface energies reflect the presence of an ultrathin adsorbed film.[18] However, there is yet no

available data or theoretical work along these lines for liquid microstructures confined by hydrophobic boundaries, which can strongly affect the precursor film.

The liquid surface is triangulated by a fine mesh and the total energy of the system is expressed as a function of the vertex coordinates comprising the surface discretization. Both the numerical methods of steepest descent and conjugate gradients are implemented. Constraints may be applied to points, lines, areas and volumes. Boundary condition parameters can be included in the optimization process.

The equilibrium shape of a liquid droplet on a homogeneous surface is a spherical cap. In the absence of surface defects and chemical inhomogeneities, the contact angle θ along the liquid–solid contact line is constant (the so-called natural contact angle) and determined by Young's law according to $\gamma_{sv} - \gamma_{sl} = \gamma_{lv} \cos \theta$. When the natural contact angle $\theta \geq \pi/2$, the liquid is said to be nonwetting; when $0 < \theta < \pi/2$, the liquid is "partially wetting." For liquid-on-solid systems in which θ is zero, the liquid is said to "completely wet" the solid surface. If $\gamma_{sv} - \gamma_{sl} > \gamma_{lv}$, the force balance expressed by Young's equation ceases to hold. For an extensive review the reader is referred to Ref. 19.

The behavior of a droplet residing on an inhomogeneous surface is somewhat more complicated. As an example, consider the case of a partially wetting droplet on a surface which presents both hydrophilic and hydrophobic patches. If the size of the patches is smaller or comparable to the droplet radius, then the contact angle will vary along the liquid–solid contact line. If the patches are significantly larger than the droplet radius, then the liquid will assume the natural contact angle appropriate to Young's equation for the relevant surface patch. For surfaces on which there exists a large contrast in natural contact angle (e.g., water in the presence of hydrophilic and hydrophobic regions), the droplet will migrate to the regions of low natural contact angle and avoid regions with large natural contact angle.[9] This applies exactly for our experiments performed with glycerol on patterned silicon surfaces.

Curved interfaces give rise to a local increase in the hydrostatic pressure inside the liquid according to the Laplace–Young equation $\Delta p = J \gamma_{lv}$, where J is the mean interface curvature. Consequently, the equilibrium shapes of a liquid are characterized by a globally constant mean curvature and a uniform increase of pressure Δp, which is proportional to the surface tension γ_{lv}.

A. Straight lines

A free liquid cylinder of sufficient length is unstable to break up into droplets, which can be observed for instance in a jet of water emanating from a tap. This instability is due to surface tension: capillary breakup occurs when the total surface area of all the droplets combined is smaller than that of the continuous jet. Using linear stability theory, Rayleigh[20] showed that a liquid jet is unstable to infinitesimal axisymmetric disturbances whose wavelength λ exceeds the circumference of the undisturbed jet.

Recent interest has focused on the stability of a thread of liquid resting on a homogenous surface, since the attractive forces between a liquid and solid may provide an additional
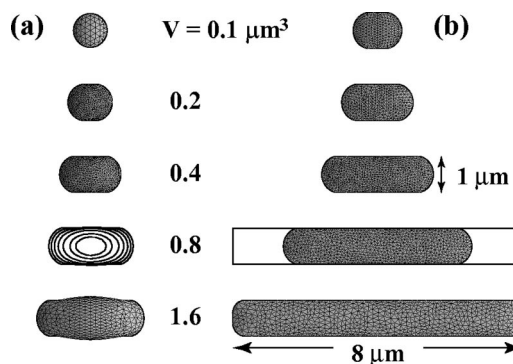

FIG. 2. Top-view profiles of liquid droplets residing on a hydrophilic rectangular strip of dimensions 1 μm $\times$ 8 μm surrounded by completely hydrophobic regions (i.e., $\theta = 180°$). The natural contact angle of the liquid on the interior region was chosen as $\theta = 60°$ for column (a) and $\theta = 30°$ for column (b). Within each column, the volume of liquid increases from 0.1 to 1.6 μm^3 as indicated by the inset labels. The droplet shape corresponding to $\theta = 60°$ and a volume of 0.8 μm^3 is presented as a contour plot with contour levels at 0, 0.1, 0.2, 0.3, 0.4, 0.5, and 0.56 μm.

stabilizing factor.[21–24] The behavior of liquid lines depends on the boundary condition at the contact line. If the contact line is immobilized or pinned, Davis[21] and Schiaffino *et al.*[23] have shown that a liquid line is unconditionally stable to small disturbances provided the contact angle is below 90°. For a thread which assumes a fixed contact angle (or one that varies smoothly with the contact line velocity), breakup can occur and the wavelength delimiting the stable region varies with the contact angle.[21,23] Gau *et al.*[25] have investigated the equilibrium shape of a liquid confined to hydrophilic stripes with a natural contact angle of zero. They find that when the liquid volume per unit length exceeds a threshold value, the minimum energy state corresponds to a liquid thread containing a single bulge. In what follows, we study the more general case, when both the natural contact angle of the liquid on the hydrophilic channel surface and the volume per unit length of the liquid line are varied, and the liquid is free to cross or recede from the channel boundaries.

One of the most elementary configurations to consider is a liquid droplet placed on a rectangular hydrophilic patch. Figure 2 shows the calculated profiles for a liquid with a natural contact angle of (a) $\theta = 60°$ and (b) $\theta = 30°$ residing on a channel measuring 1 μm $\times$ 8 μm. The exterior of the channel presents a completely hydrophobic surface ($\theta = 180°$). The volume deposited increases from 0.1 to 1.6 μm^3. For the larger contact angle but smallest volume, the liquid assumes the shape of a spherical cap. The droplet does not sense the channel boundaries and behaves as if residing on a homogeneous surface. As the volume is increased, the contact line migrates toward the channel boundaries and along the stripe, but remains confined to the hydrophilic interior region. For even larger volumes, the liquid with the lower contact angle covers essentially the entire channel; however, the liquid with $\theta = 60°$ forms a bulge, which becomes more pronounced with increasing volume. The presence of the bulge (or lack of complete wetting of the hydrophilic strip) signals that the loss in liquid–vapor surface energy exceeds the gain in liquid–solid contact energy.
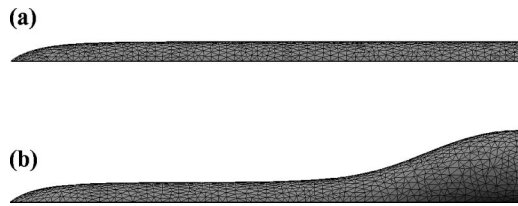
(a)

(b)

FIG. 3. Side-view profiles of liquid lines with a natural contact angle of $\theta = 30°$ on a hydrophilic stripe of dimensions 1 μm$\times$16 μm surrounded by a completely hydrophobic surface. The liquid volume is increased from (a) 3.2 μm^3 to (b) 6.4 μm^3.
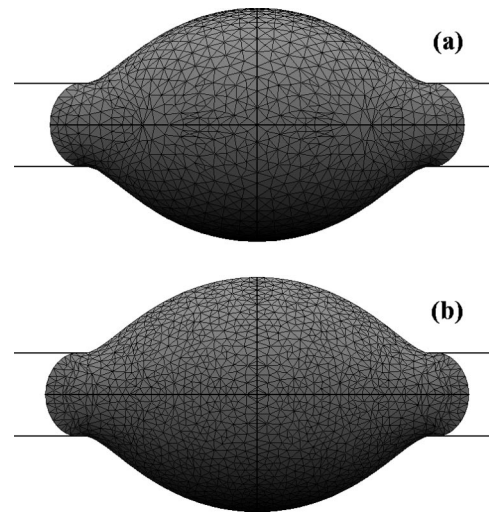

(a)

(b)

FIG. 4. Top-view profiles of droplets on a hydrophilic channel surrounded by regions of a less hydrophilic surface. The natural contact angle of the liquid on the interior and exterior regions is (a) 40° and 95° and (b) 30° and 75°.

The formation of a bulge is not unique to liquids which have a large natural contact angle on a surface. For example, Fig. 3 shows a comparison of side views of two different volumes of liquid with $\theta = 30°$ on a rectangular stripe with dimensions 1 μm$\times$16 μm. Since the profiles are mirror symmetric, only the left half of the surface profile is shown. For a volume of $V = 3.2 \ \mu$m^3 the liquid extends over the entire lane and assumes a rather even height profile [Fig. 3(a)], except at the left edge. When the volume is doubled, the surface exhibits a pronounced bulge [Fig. 3(b)]. Interestingly, the profile of the flat portion in Fig. 3(b) is nearly the same as in Fig. 3(a). The shape and distribution of liquid on a finite channel therefore depends critically not only on the contact angles and surface tensions involved, but also on the volume of liquid deposited.

If the amount of liquid deposited on a long channel is subcritical, in the sense that its volume per unit length is smaller than the area of a circular sector corresponding to the channel width w and the liquid's natural contact angle θ, then the contact lines will recede to the stripe interior and the liquid will behave as if residing on a homogeneous substrate. This critical volume condition is expressed by

$$V/l < \frac{w^2}{4\sin^2\theta}\left(\theta - \frac{1}{2}\sin 2\theta\right), \tag{1}$$

where l is the length of the lane and θ is given in radians. In this case, a liquid thread does not sense the channel boundaries and hence is susceptible to capillary breakup as discussed above. If V/l is increased above the critical value, the contact angle increases above its natural value on a homogeneous surface. This stabilizes the line against capillary breakup[21–24] until either bulge formation occurs or until the angle exceeds the equilibrium value on the hydrophobic exterior. In the latter case the liquid spreads beyond the channel boundaries. Since the natural contact angles on a sample are never exactly constant and homogeneous, the liquid will cross the channel edges at the position of a local minimum of the exterior contact angle.

For the simulations shown in Figs. 2 and 3, the region exterior to the hydrophilic patch is completely nonwetting. It is therefore energetically unfavorable for the liquid to migrate into these regions. When the exterior is rendered partially wetting, a liquid bulge may advance into this region in an effort to minimize the total energy. This behavior is shown in Fig. 4, in which both natural contact angles on the interior and exterior portions are varied. Figure 4 depicts the equilibrium configuration for: (a) $\theta_{\text{interior}} = 40°$ and θ_{exterior}

$= 95°$ and (b) $\theta_{\text{interior}} = 30°$ and $\theta_{\text{exterior}} = 75°$. Although the contrast in angles is larger in (a), the perimetral profiles are very similar. Close inspection reveals slightly steeper profiles along the edges in Fig. 4(a), but that would be difficult to discern experimentally from this perspective. This example leads to the unfortunate conclusion that the contact angles cannot be extracted unambiguously from top view profiles, as would be observed in an optical microscope. For droplets larger than approximately 20 μm, evanescent wave microscopy can be used to measure the perimetral shape and location of the contact line.[25]

B. Rings and loops

An interesting class of patterns are liquid structures in the shape of horizontal sections of a circular torus (donut-shaped rings). Provided the solid substrate presents a homogeneous, partially wetting surface which allows free, unconstrained migration, a liquid ring will be unstable to shrinkage into a single central droplet. If the width of the liquid filament, however, is substantially smaller than the diameter of the overall ring structure, then it is possible that the liquid ring undergoes capillary breakup on a time scale faster than that required for shrinkage to a single droplet. In the case of a Newtonian liquid, the time scale for the redistribution during capillary breakup is controlled by the ratio $\mu R / \gamma_{\text{lv}}$, where μ is the liquid's viscosity and R is the halfwidth of the liquid filament. The final configuration would then be a series of droplets distributed along the positions of the original ring.

If the shrinkage of the liquid ring toward a central drop is impeded by a hydrophobic patch, the situation for breakup may be similar. According to the Rayleigh criterion, the two competing length scales which determine the propensity for capillary breakup are the overall length of the liquid filament (which in this case is the overall ring circumference) and the radius of curvature of the liquid rim in cross section.
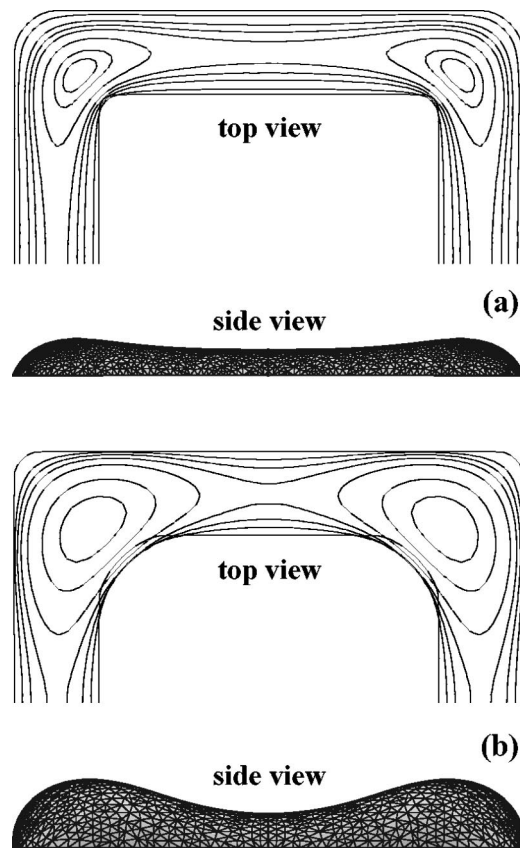
FIG. 5. Top- and side-view profiles for two different volumes of liquid on a hydrophilic channel forming a square loop of 1 μm width. The top view (a) depicts the equilibrium shape for 5 μm^3, the bottom view (b) for 10 μm^3. In both examples, the contact angle on the channel was chosen to be 45° and the exterior angle 135°. Only half of the entire loop is shown in top view. The contour levels are: (a) 0.01, 0.1, 0.2, 0.25, 0.29, 0.35, 0.4 and 0.42 μm, and (b) 0.01, 0.2, 0.3, 0.39, 0.5, 0.65, 0.75 μm.

In Fig. 5 we show top and side views of liquid profiles on a hydrophilic square-shaped loop 1μm wide. The length of the interior square is 4 μm. Only half the square loop is shown due to the inherent mirror symmetry. The contact angle on the channel was chosen to be 45° and the exterior angle 135°. The difference between the upper and lower profiles is the amount of volume V deposited. Figure 5(a) presents the case of $V = 5$ μm^3, while in Fig. 5(b) $V = 10$ μm^3. The liquid loop is in good registry with the surface patterns for the smaller volume; however, the side view indicates a slightly thicker rim at the corners. As seen in Fig. 5(b), these bulges become more pronounced as the volume is increased. Moreover, the edge definition of the inner corners of the square loop becomes worse. These studies indicate that the pattern printed on a target substrate will not maintain fidelity with the original pattern if it contains corners and loops, and if the deposited volume is too large.

C. Varying strip widths

Typically, several length scales coexist in the layout of electronic microdevices. The contact or bonding pads are in the 100 μm range, whereas the current leads are in the micron range and the actual devices can be smaller than 1 μm. Since smaller dimensions automatically involve smaller radii
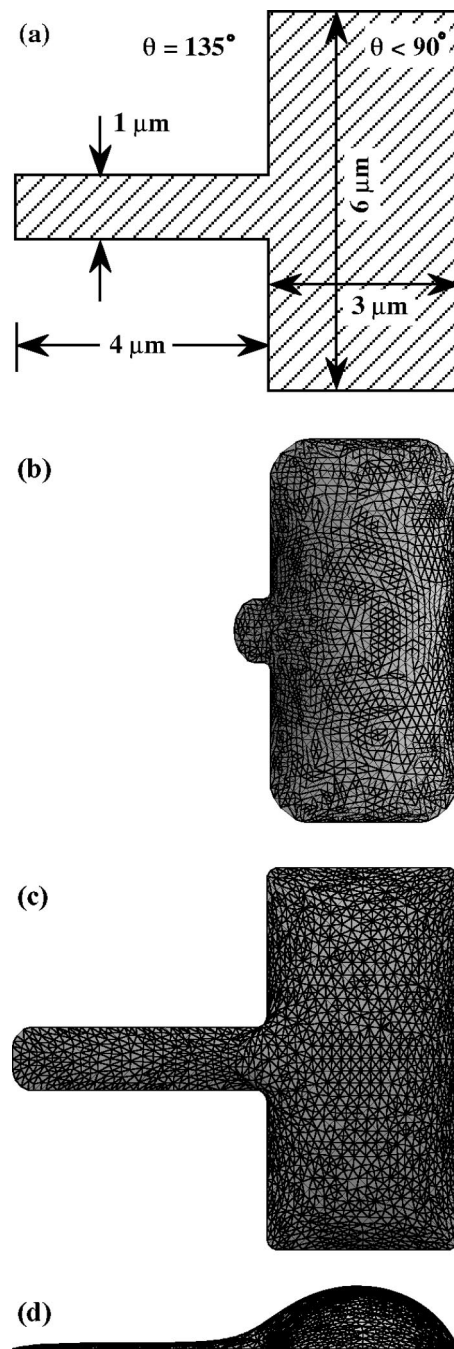

FIG. 6. Top- and side-view profiles of a 9.7 μm^3 liquid drop on a hydrophilic rectangular pad with a narrower appending hydrophilic patch. The imposed surface pattern is sketched in (a). In (b)–(d) top views for a liquid with a interior natural contact angle of (b) 30° and (c) 10° are depicted. In (d) the side view corresponding to (c) is presented.

of curvature R_i, the associated local increase in Laplace pressure of the liquid structures drives the liquid out of regions with smaller feature sizes.

In Fig. 6 we present profiles of liquid droplets on a hydrophilic surface pattern composed of two connected rectangles [see Fig. 6(a)], one of which is broad and the other narrow. The natural contact angle on the hydrophobic exterior region was chosen to be 135° and the liquid was free to cross boundaries. The liquid volume is 9.7 μm^3. For $\theta = 30°$ [Fig. 6(b)] or higher, the liquid almost completely
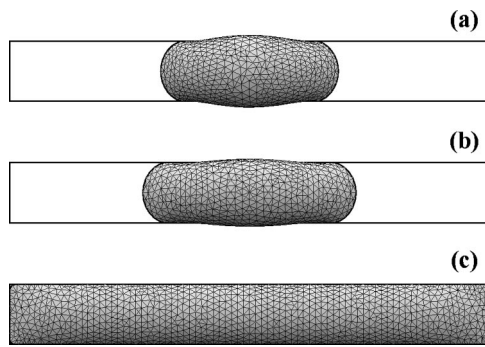
FIG. 7. Shape changes of a liquid droplet on a hydrophilic channel for different surface tensions but constant volume. The stripe has dimensions 1 μm $\times$ 8 μm and is surrounded by completely hydrophobic regions. In (a) the droplet profile for a natural contact angle of 60° is depicted. In (b) and (c) the influence of a surfactant is illustrated, which reduces the surface tension by (b) 20% and (c) 50% rendering the liquid completely wetting and enhancing the edge definition.

recedes from the narrow rectangle. For $\theta = 10°$ [Fig. 6(c)], the liquid almost covers the entire surface shape. As is to be expected, a liquid with smaller natural contact angle wets the available hydrophilic surface area more effectively. Inspection of the side view corresponding to the latter case [Fig. 6(d)], however, is disappointing, since the majority of the liquid remains on the larger rectangle, with only a thin film protruding into the narrow section. Such an unbalanced height profile is highly undesirable for the printing process, since only the liquid on the broad rectangle would be transferred, but not the liquid on the narrow one.

D. Influence of surfactant additive

The preceding sections have shown that surface tension may induce nonuniformities in the liquid surface profiles. While the contact energy between the liquid and the hydrophilic channel surface tends to spread the liquid over the entire defined pattern, surface tension can induce a recession from narrower parts, or an unwanted accumulation in bulges. One way to reduce these effects is the addition of an insoluble surfactant, which reduces the surface tension without changing the liquid–solid contact energy.

In Fig. 7 we compare top view profiles of a liquid droplet of variable surface tension on a rectangular hydrophilic patch. The region exterior to the patch is completely hydrophobic, thereby discouraging any migration beyond the channel boundaries. If the liquid droplet has a high surface tension such that it maintains a natural interior contact angle of 60°, it will not spread into all the available lateral area but form a bulge whose overall surface area is lowest [Fig. 7(a)]. This is the same behavior observed in Fig. 2. When the tension is reduced by 20% but the volume held constant, the shape elongates noticeably [Fig. 7(b)]. For a reduction in surface tension of 50%, the liquid covers the entire hydrophilic region [Fig. 7(c)]. According to Young's equation, the reduction of the surface tension is accompanied by a corresponding decrease of the contact angle. The undesirable rounding-off of liquid in a corner and the recession from the end regions of a channel can therefore be reduced by addi-
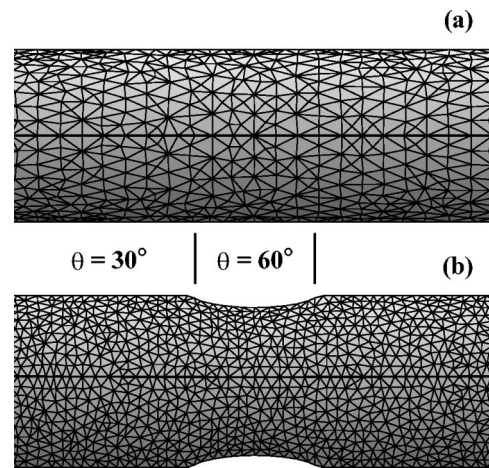

FIG. 8. Top-view profiles of a liquid line of natural interior angle $\theta = 30°$ resting on a hydrophilic lane of 1 μm width. The small region between the two vertical lines represents a chemical defect of dimensions 1 μm $\times$ 0.7 μm where the natural interior contact angle is increased to $\theta = 60°$. The deposited volumes are (a) 0.3 μm^3 and (b) 0.19 μm^3 per unit length (in μm).

tion of a surfactant. Such an additive is expected to enhance edge definition and pattern fidelity in the printing process.

E. Topological or chemical defects

An issue of significant technological importance is the influence of chemical and topological defects on the shape of liquid microstructures. While chemical defects may be due to adsorption of surface contaminants, which can locally modify a liquid's natural contact angle, topological defects can arise from imperfections in the mask used for the photolithography process. In our experimental studies we have observed that mask imperfections can induce local boundary indentations and thus linewidth fluctuations of the hydrophilic channels.

In Fig. 8, we examine the behavior of two liquid threads with different volumes on a 1 μm wide hydrophilic channel. The liquid has a natural interior angle of 30° along the majority of the hydrophilic patch except for a small "contaminated" portion where the angle is assumed to be 60°. The contaminated rectangular portion measures 1 μm $\times$ 0.7 μm. The liquid volume per unit length (in μm) in Fig. 8(a) is 0.3 μm^3 and in Fig. 8(b) is 0.19 μm^3. For the larger volume where the sidewall slope of the liquid profile is close to or above its natural contact angle on the contaminating patch, the liquid profile does not reflect the presence of the defect area. Clearly this can occur only if the difference between the contact angles on the lane and the contaminating patch is not too large. When the liquid volume is reduced—as might occur by evaporation—the contaminated area induces a local narrowing of the liquid line as shown in Fig. 8(b). This local shrinkage constitutes the onset of capillary breakup. If the volume is reduced further, the transverse radius of curvature decreases. This reduction leads to an increased Laplace pressure in the center of the patch, which cannot be balanced by the associated negative curvature along the line. Hence the liquid will be driven out of the patch area leading to pinch
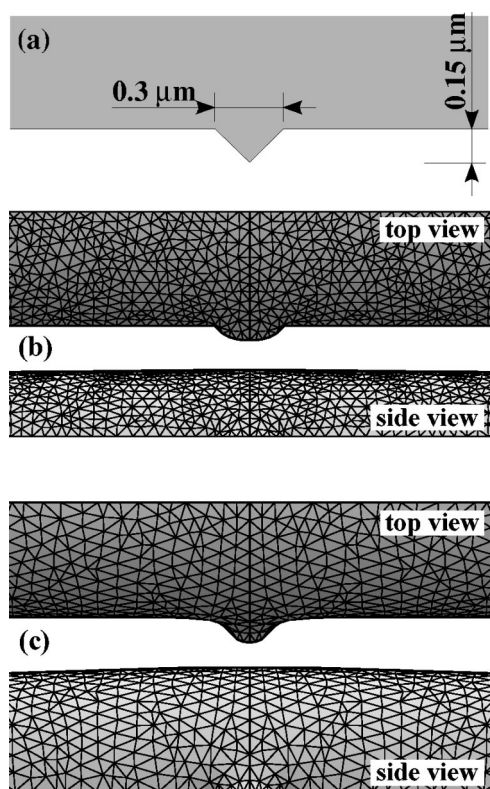
FIG. 9. Top- and side-view profiles of a liquid line on a hydrophilic channel of 1 μm width containing a triangular topological defect. The defect consists of a local protrusion of the channel boundary in the shape of an equilateral triangle with an apex angle of 90°. The distance between the apex of the protrusion and the remaining channel boundary (the height of the triangle) is 0.15 μm. The deposited volumes are: (b) 0.2 μm^3 and (c) 0.4 μm^3 per unit length (in μm). Only half of the liquid structure is shown in top view. In the vicinity of the inner corners of the triangle in (c), the liquid profile slightly overhangs and the top view does not show the actual liquid–solid contact line.

off. A local decrease of the channel width has the same effect and can provide an inhomogeneity which initiates capillary breakup.

In Fig. 9, we present profiles of liquid lines on a 1 μm wide channel, which has a protrusion in the shape of an equilateral triangle with an apex angle of 90°. In each case shown, there is enough liquid to cover the entire hydrophilic region. The distance between the apex of the protrusion and the undisturbed lane boundary (i.e., the height of the triangle) is 0.15 μm and its base length is 0.3 μm [see Fig. 9(a)]. The liquid volume per unit lane length (in μm) shown in Fig. 9(b) 0.2 μm^3 and in Fig. 9(c) is 0.4 μm^3. For both volumes, the triangular area is not entirely wetted by the liquid. The apex is devoid of fluid since the cost of increasing the surface area would exceed the gain due to an increase of interfacial contact energy in the total energy balance.

This situation can be viewed in terms of a frequency filter. The liquid contact line acts as a low pass filter of the channel boundary when the modulation of the latter occurs on a length scale smaller than the channel width. If the boundary line fluctuations are comparable to the channel width, however, then bulges will form in regions of increased channel width and significantly alter the surface profile of the liquid thread. A faint increase in the liquid height

is already visible in Fig. 9(c). If more liquid were added, the bulge would become more pronounced.

IV. DISCUSSION

In Sec. III, we explored through simulations the equilibrium shape of liquid microstructures residing on inhomogeneous surfaces containing hydrophilic and hydrophobic regions. The computed shapes closely resemble the liquid conformations obtained experimentally for glycerol on OTS patterned silicon wafers as presented in Fig. 1. Our results show that the use of liquids for high resolution lithography has both advantageous and undesirable aspects. For example, liquid contact lines smooth channel boundary irregularities, such as those arising from imperfections in the original photolithographic mask. On the other hand, capillary breakup and bulge formation need to be controlled, which in general requires the proper adjustment of the deposited liquid volume. Capillary breakup can be discouraged by decreasing the liquid's natural contact angle on the hydrophilic regions. The tendency of bulge formation can be reduced by suitable placement of small hydrophobic patches at positions where bulges tend to nucleate. However, this approach requires lithographic control on a length scale much smaller than the designed minimum linewidth and is thus technologically demanding.

Reducing the liquid's surface tension by a surfactant additive can improve the edge resolution of the printing process. In view of the results shown in Fig. 7, a decrease of surface tension increases the ratio of the wetted to bare surface area on the hydrophilic regions. Unfortunately, this solution does not completely alleviate the problem of uneven height profiles, which is associated with the presence of disparate length scales (see Fig. 6). Furthermore, the beneficial effect of increased edge definition counteracts the smoothing of boundary line irregularities due to mask imperfections, which was discussed in Sec. III E.

Therefore, we deduce the general design rule that the liquid pattern to be printed and transferred should not contain very different length scales, such as combinations of broad and narrow rectangles as depicted in Fig. 6(a). Even if these regions are not directly connected, the liquids adhering to them will maintain different thicknesses, which will ruin the possibility of even liquid transfer upon printing. As a workaround to this difficulty, we propose the discretization of the pattern into closely spaced squares or rectangles of identical size or linewidth, which are separated by narrow hydrophobic spacers. All individual patches would then have the same dimensions and the liquid height profiles would be identical throughout the entire patterned area, thus maintaining regularity and uniformity between different parts during the transfer process. When printing such a droplet array onto another surface, the isolated droplets would coalesce, thus removing the artificial discretization of the desired pattern on the substrate.

In this article we have investigated the equilibrium conformation of liquid microstructures on a patterned surface for various shapes, volumes and surface energies. Questions related to the time scale of surface tension driven processes or

to the rheological properties of the liquid-like viscoelasticity or thixotropy cannot be considered within this framework. In the actual technological process, the interplay between viscous and capillary effects determines the time scale at which equilibrium is approached. Therefore, it may be possible to suppress undesirable instabilities like capillary breakup and bulge formation by optimizing the dynamical material parameters. The study of the associated dynamics will be the next step in our investigation of wet printing at the microscale.

ACKNOWLEDGMENTS

[1] A. Kumar and G. Whitesides, Appl. Phys. Lett. **63**, 2002 (1993).

[2] R. J. Jackman, J. L. Wilbur, and G. M. Whitesides, Science **269**, 664 (1995).

[3] Y. Mikami *et al.*, IEEE Trans. Electron Devices **41**, 306 (1994).

[4] H. A. Biebuyck, N. B. Larsen, E. Delamarche, and B. Michel, IBM J. Res. Dev. **41**, 159 (1997).

[5] L. Libioulle, A. Bietsch, H. Schmid, B. Michel, and E. Delamarche, Langmuir **15**, 300 (1999).

[6] J.-P. Bourgoin and S. Palacin, Langmuir **14**, 3967 (1998).

[7] J. Drelich, J. L. Wilbur, J. D. Miller, and G. M. Whitesides, Langmuir **12**, 1913 (1996).

[8] A. Paterson and M. Fermigier, Phys. Fluids **9**, 2210 (1997).

[9] L. W. Schwartz and R. R. Eley, J. Colloid Interface Sci. **202**, 173 (1998).

[10] L. W. Schwartz, Proceedings of the Third European Coating Symposium, Erlangen, September 1999.

[11] J. B. Brzoska, I. Ben Azouz, and F. Rondelez, Langmuir **10**, 4367 (1994).

[12] S. R. Wasserman, G. M. Whitesides, I. M. Tidswell, B. M. Ocko, P. S. Pershan, and J. D. Axe, J. Am. Chem. Soc. **111**, 5852 (1989).

[13] C. S. Dulcey, J. H. Georger, V. Krauthamer, D. A. Stenger, T. L. Fare, and J. M. Calvert, Science **252**, 551 (1991).

[14] K. J. Ruschak, Annu. Rev. Fluid Mech. **17**, 65 (1985).

[15] *Handbook of Chemistry and Physics*, edited by R. C. Weast and M. J. Astle (Chemical Rubber Corp., Boca Raton, IL, 1982).

[16] K. Brakke, Exp. Math. **1**, 141 (1992).

[17] J. Drelich, Colloids Surf., A **116**, 43 (1996).

[18] D. Li and A. W. Neumann, Adv. Colloid Interface Sci. **36**, 125 (1991).

[19] P. G. de Gennes, Rev. Mod. Phys. **57**, 827 (1985).

[20] Lord Rayleigh, Proc. R. Soc. London, Ser. A **10**, 4 (1879).

[21] S. H. Davis, J. Fluid Mech. **98**, 225 (1980).

[22] K. Sekimoto, R. Oguma, and K. Kawasaki, Ann. Phys. **176**, 359 (1987).

[23] S. Schiaffino and A. A. Sonin, J. Fluid Mech. **343**, 95 (1997).

[24] R. V. Roy and L. W. Schwartz, J. Fluid Mech. **391**, 293 (1999).

[25] H. Gau, S. Herminghaus, P. Lenz, and R. Lipowsky, Science **283**, 46 (1999).